Dynamics and Thermodynamics of the Regulatory Domain of Human Cardiac Troponin C in the Apo- and Calcium-Saturated States†

Leo Spyracopoulos, Stéphane M. Gagné, Monica X. Li, and Brian D. Sykes*

MRC Group in Protein Structure and Function, Department of Biochemistry, University of Alberta, Edmonton, Alberta, T6G 2H7, Canada

Received July 15, 1998; Revised Manuscript Received October 23, 1998

ABSTRACT: The contraction of cardiac and skeletal muscles is triggered by the binding of Ca^{2+} to their respective troponin C (TnC) proteins. Recent structural data of both cardiac and skeletal TnC in both the apo and Ca^{2+} states have revealed that the response to Ca^{2+} is fundamentally different for these two proteins. For skeletal TnC, binding of two Ca^{2+} to sites 1 and 2 leads to large changes in the structure, resulting in the exposure of a hydrophobic surface. For cardiac TnC, Ca^{2+} binds site 2 only, as site 1 is inactive, and the structures show that the Ca^{2+}-induced changes are much smaller and do not result in the exposure of a large hydrophobic surface. To understand the differences between regulation of skeletal and cardiac muscle, we have investigated the effect of Ca^{2+} binding on the dynamics and thermodynamics of the regulatory N-domain of cardiac TnC (cNTnC) using backbone ^{15}N nuclear magnetic resonance relaxation measurements for comparison to the skeletal system. Analysis of the relaxation data allows for the estimation of the contribution of changes in picosecond to nanosecond time scale motions to the conformational entropy of the Ca^{2+}-binding sites on a per residue basis, which can be related to the structural features of the sites. The results indicate that binding of Ca^{2+} to the functional site in cNTnC makes the site more rigid with respect to high-frequency motions; this corresponds to a decrease in the conformational entropy ($T\Delta S$) of the site by 2.2 kcal mol^{-1}. Although site 1 is defunct, binding to site 2 also decreases the conformational entropy in the nonfunctional site by 0.5 kcal mol^{-1}. The results indicate that the Ca^{2+}-binding sites in the regulatory domain are structurally and energetically coupled despite the inability of site 1 to bind Ca^{2+}. Comparison between the cardiac and skeletal isoforms in the apo state shows that there is a decrease in conformational entropy of 0.9 kcal mol^{-1} for site 1 of cNTnC and little difference for site 2.

Initiation of contraction of cardiac and skeletal muscle occurs via Ca^{2+} binding to the regulatory domain of the thin filament protein TnC[1] (for reviews, see refs *1*−*5*). The Ca^{2+} signal is believed to initiate a succession of protein structural changes and altered protein−protein interactions within the thin filament that allows for the interaction of myosin with actin, and ultimately leads to muscle contraction. TnC in skeletal and cardiac muscle is an ∼160 residue, highly α-helical protein consisting of two similarly sized domains that are joined by a central helix that is flexible in solution (*6*−*8*). Each domain contains two E−F hand helix-loop-helix motifs, which can potentially bind two Ca^{2+} ions. The role of the E−F hands in the C-domain (sites 3 and 4) is believed to be structural (*9*), while Ca^{2+} binding to the E−F hands in the N-domain (sites 1 and 2) serves a regulatory purpose (*1, 10*−*12*). In cardiac muscle, contraction occurs with Ca^{2+} binding to site 2 only, whereas contraction in skeletal muscle requires Ca^{2+} binding to both sites 1 and 2 (*10, 11*).

The Ca^{2+}-induced structural transition in sTnC has been elucidated with the description of the NMR solution structures of the sNTnC in the apo- and Ca^{2+}-saturated states (*13*), the X-ray structure of $(Ca^{2+})_2$ sTnC (*6, 7, 14*), and the NMR solution structure of $(Ca^{2+})_4$ sTnC (*8*). These structures have been complemented with the recently determined crystal structures of Ca^{2+}-saturated sNTnC (*15*) and $(Ca^{2+})_4$ sTnC (*16*). These structural studies have shown that the Ca^{2+}-induced structural transition in sNTnC involves large interhelical movements and the accompanying exposure of a hydrophobic patch which is believed to serve as an interface for subsequent protein−protein interactions between sTnC and sTnI. The recently determined NMR solution structures of apo- and Ca^{2+}-saturated cNTnC (*17*) and Ca^{2+}-saturated cTnC (*18*) have shown that, in contrast to sTnC, the regulatory domain of cTnC does not undergo an opening in response to Ca^{2+}. The sequence of cTnC is 70% identical to that of sTnC; however, there are critical sequence differences in the first forty residues of cTnC compared to sTnC (*19*). Specifically, Ca^{2+}-binding site 1 (residues 29−40) is defunct on account of differences between two Ca^{2+} coordinating ligands (D29L, D31A) and an insertion (Val-28) compared to sTnC. Similarly, the engineered mutant E41A-sNTnC does

† Supported by the MRC Group in Protein Structure and Function, and the Heart and Stroke Foundation of Canada. L.S. is a Heart and Stroke Foundation of Canada Research Fellow.

* To whom correspondence should be addressed. E-mail: brian.sykes@ualberta.ca.

[1] Abbreviations: (N or C)TnC, (N- or C-) terminal domain of troponin C; (s or c)TnC, (skeletal or cardiac) troponin C; (s or c)TnI, (skeletal or cardiac) troponin I; HSQC, heteronuclear single quantum coherence; HMQC, heteronuclear multiple quantum coherence; NMR, nuclear magnetic resonance; NOE, nuclear Overhauser effect; RMSD, root-mean-square deviation.

10.1021/bi9816960 CCC: $15.00
Published on Web 12/05/1998

not undergo a structural opening in response to Ca^{2+} due to the inability of site 1 in this mutant to respond to Ca^{2+} (*20*). These studies underscore the importance of Ca^{2+} binding to site 1 for the opening of troponin C.

The NMR solution and X-ray crystal structures provide critical insight into the final states of the Ca^{2+}-binding event (apo- vs Ca^{2+}-saturated). However, these structures do not provide details on the dynamics, thermodynamics, and energetics of the Ca^{2+}-induced structural changes. Recently, Ca^{2+} titrations of sNTnC, E41A-sNTnC, and cNTnC were followed in detail by monitoring changes in two-dimensional $\{^1H,^{15}N\}$-HMQC and $\{^1H,^{15}N\}$-HSQC NMR spectra (*21, 22*). These experiments showed that Ca^{2+} binding to sNTnC occurs in a stepwise manner, and that the Ca^{2+} affinity for site 2 is 10-fold greater than that for site 1 ($K_{D2} \sim 1.7$ μM, $K_{D1} \sim 16$ μM). For E41A-sNTnC, the Ca^{2+} affinity for site 1 is greatly reduced ($K_{D1} \sim 1300$ μM) and the affinity for site 2 is also reduced ($K_{D2} \sim 15$ μM). For cNTnC, the dissociation constant for Ca^{2+} binding to site 2 was found to be 2.6 μM. These results clearly indicate that sites 1 and 2 are energetically coupled and provide mechanistic details that are not available from structural data.

Backbone amide ^{15}N NMR relaxation measurements have provided detailed insight into the rotational and internal dynamics of proteins (*23*−*25*). Relaxation data are often interpreted within the context of the Lipari-Szabo model-independent formalism, from which an overall rotational correlation time, an internal correlation time, and an order parameter (S^2) can be obtained for a given backbone amide N−NH vector in a protein or peptide (*26*−*28*). The strength of this approach is based on the fact that S^2 is a function of the amplitude of internal motion and can be interpreted in the absence of a specific motional model. The order parameter can be equated to the orientational probability distribution of a N−NH vector and can therefore be expressed as a function of thermodynamic parameters such as entropy and enthalpy (*29*−*31*).

In a recent paper, we have shown that the contribution to the conformational entropy derived from motions sensed by ^{15}N NMR relaxation measurements differs by approximately 1 kcal mol^{-1} between sites 1 and 2 of sNTnC (*32*). This is close to the difference in free energy of binding between the two sites. In this paper, we have used backbone amide ^{15}N NMR relaxation measurements of apo- and Ca^{2+}-saturated cNTnC to directly determine the contribution of conformational entropy changes in picosecond to nanosecond time scale motions of sites 1 and 2 to the free energy of Ca^{2+} binding to cNTnC in order to provide insight into the entropic differences between the skeletal and cardiac proteins which respond so differently in a structural fashion to Ca^{2+} binding.

MATERIALS AND METHODS

Sample Preparation. The expression vector for cNTnC (1−89) was engineered as described previously (*33*). ^{15}N-labeled protein was expressed in *Escherichia coli* as previously described (*21, 34*). Purification of the protein was achieved using previously described protocols employed for cleaved sTnC (*35*). cNTnC was obtained in the apo state as previously described for sNTnC (*21*). NMR samples contained 500 μL of 9:1 H_2O/D_2O (pH 6.7), 100 mM KCl, 15 mM DTT, 5 mM EDTA, and 1.78 mM protein for apo-cNTnC. Ca^{2+}-saturated samples of cNTnC contained 1.3 mL of 9:1 H_2O/D_2O (pH 6.7), 100 mM KCl, 15 mM DTT, 1 mM Ca^{2+}, and ∼0.15 mM protein. All NMR samples contained 0.03% NaN_3.

NMR Spectroscopy. NMR spectra were acquired using Varian Unity INOVA 500 MHz or Unity 600 MHz spectrometers equipped with 5 mm triple resonance probes and *z*-axis pulsed field gradients and a Varian Unity 300 MHz spectrometer with a 5 mm inverse broadband probe for apo-cNTnC. For the Ca^{2+}-saturated protein, NMR spectra were acquired on a Unity INOVA 500 MHz spectrometer equipped with an 8 mm triple resonance probe with *z*-axis pulsed field gradients. ^{15}N-T_1, ^{15}N-T_2, and $\{^1H\}^{15}N$ NOE experiments were conducted at 30 °C using sensitivity-enhanced gradient pulse sequences developed by Farrow et al. (*36*) at 500 and 600 MHz and sensitivity-enhanced nongradient pulse sequences at 300 MHz written in-house (L. Spyracopoulos) that are modified versions of sequences developed by Kördel et al. (*37*) (Figures S1−S3). For the apo-protein, T_1 data were acquired once at 300, 500, and 600 MHz using relaxation delays of 11.1, 55.5, 122.1, 199.8, 277.5, 388.5, 499.5, 666.0, 888.0, and 1254.3 ms. Pulse sequence details are given in Tables S1 and S2, and all other details are as previously described (*36*). ^{15}N-T_2 data was acquired once at 300 MHz using delays of 16.6, 33.2, 49.7, 66.3, 82.9, 99.5, 116.1, and 132.6 ms, once at 500 MHz using delays of 16.6, 33.2, 49.8, 66.4, 83.0, 99.7, 116.3, 132.9, 149.5, and 166.1 ms, and once at 600 MHz using delays of 16.3, 32.6, 48.9, 65.2, 81.4, 97.7, 114.0, 130.3, 146.6, and 162.9 ms. For the T_2 pulse sequence, the delay between transients was 3 s at 500 MHz and 2.5 s at 300 and 600 MHz, which, in conjunction with the field strength of nitrogen pulses and decoupling, drastically reduces the effect of dielectric sample heating due to the radio frequency field, as noted previously (*32*). Details for the acquisition of T_2 data for apo-cNTnC are given in Tables S1 and S2. $\{^1H\}^{15}N$ NOEs were measured by recording spectra in the presence and absence of proton saturation. The spectrum recorded without proton saturation was acquired with a delay between transients of 8 s at 300 MHz and 5 s at 500 and 600 MHz. The spectrum recorded in the presence of proton saturation incorporated a relaxation delay of 4.5 s, followed by 3.5 s of proton saturation for a total delay between transients of 8 s at 300 MHz. The 500 and 600 MHz spectra recorded in the presence of proton saturation incorporated a relaxation delay of 2 s, followed by 3 s of proton saturation, for a total delay between transients of 5 s. Acquisition details are given in Tables S1 and S2 and Farrow et al. (*36*).

For the Ca^{2+}-saturated protein, T_1 data were acquired with relaxation delays of 11.1, 55.5, 122.1, 199.8, 277.5, 388.5, 499.5, 666.0, and 888.0 ms. T_2 data were acquired with relaxation delays of 16.5, 33.03, 49.54, 66.05, 82.57, 99.08, 115.60, and 132.11 ms, and a delay between transients of 2.5 s. Pulse sequence details are given in Table S3, and all other details are as in this paper and Farrow et al. (*36*). $\{^1H\}^{15}N$ NOEs were recorded in the same fashion as that used for apo-cNTnC (see Table S3 and Farrow et al. (*36*)).

Data Processing and Analysis. All spectra were processed with the program NMRPipe (*38*). The superposed orthogonal components of the sensitivity-enhanced two-dimensional free induction decays were sorted and processed with the

ranceY.M macro within the NMRPipe software. As noted previously, postacquisition processing of the t_2 interferograms for removal of residual water was not necessary (*32*), except for the ^{15}N-T_2 spectra measured at 300 MHz. For apo-cNTnC, 90°-shifted sine and sine-squared window functions were applied in t_2 and t_1, respectively. Linear prediction was employed to extend the t_1 domain by half the number of experimental points. The t_2 and t_1 domains were extended to twice the number of points with zero-filling. Baseline correction was performed with an automatic polynomial subtraction in the F_2 and F_1 domains, and the region upfield of 6.5 ppm in the F_2 dimension was discarded. The 2D {^{1}H-^{15}N}-HSQC spectrum containing the most intense resonances in a given T_1 or T_2 decay series or the {^{1}H}^{15}N NOE spectrum obtained without proton saturation was peak-picked manually with the PIPP program (*39*). All remaining peak intensities were picked automatically with the program CAPP (*39*). The entire procedure, from sorting of the FIDs to peak picking, was performed automatically using in-house written UNIX shell scripts. T_1 and T_2 values were obtained by nonlinear least-squares fits of the amide cross-peak intensities to a two-parameter exponential decay using software provided by Lewis E. Kay, except for T_1^{300} values, which were obtained from nonlinear least-squares fits of the amide cross-peak intensities to three-parameter exponential decays using the xcrvfit program (executable available at the following address: http://www.pence.ualberta.ca). Uncertainties in the measured T_1 and T_2 data were obtained from the nonlinear least-squares fits. Uncertainties in the NOE values were estimated from the baseplane noise in the 2D {^{1}H-^{15}N}-HSQC spectra recorded with and without proton saturation.

RESULTS

^{15}N-T_1, T_2, and NOE Data. The backbone amide ^{15}N and ^{1}H chemical shift assignments for apo- and Ca^{2+}-saturated cNTnC have been reported previously (*17*). For apo-cNTnC, ^{15}N NMR relaxation data for 59 of 89 residues were obtained at 300 MHz, and 72 of 89 at 500 and 600 MHz. Of the seventeen uncharacterized residues at 500 and 600 MHz, M1 and D2 were not observed due to rapid exchange with water, P52 and P54 do not have amide protons, and the remaining residues were overlapped in the 2D {^{1}H-^{15}N}-HSQC spectra. For the 300 MHz relaxation data, additional residues were excluded due to overlap and poor signal-to-noise in the 2D {^{1}H-^{15}N}-HSQC spectra. Relaxation data for the apo-protein are shown in Figures 1 and 2. The average T_1^{300} for all residues was 252 ± 41 ms with an average error of 26 ms, the average T_1^{500} for all residues was 444 ± 22 ms with an average error of 7 ms, and the average T_1^{600} was 548 ± 22 ms with an average error of 5 ms (Figure 1a). The pattern of T_1 values is similar at the three fields. Residues for which internal motion affects the measured T_1 value were identified by an NOE less than 0.49, 0.60, or 0.65 at 300, 500, and 600 MHz, respectively. These included residues 5, 7, 10, 20, 30, 33, 34, 41, 43, 56, 62, 66, and 67 at 300 MHz, residues 3−5, 7, 8, 30−34, 66, and 67 at 500 MHz, and residues 3−5, 30−34, 51, and 65−67 at 600 MHz. Most of these residues are located within the N-terminus, Ca^{2+}-binding sites, and the BC linker. Excluding these residues gives T_1^{600}/T_1^{300}, T_1^{500}/T_1^{300}, and T_1^{600}/T_1^{500} ratios of 2.2 ± 0.4, 1.8 ± 0.3, and 1.25 ± 0.07, respectively. The average T_2^{300} for all residues is 145 ± 16 ms with an average error of 7 ms, the average T_2^{500} is 145 ± 18 ms with an average error of 1 ms, and the average T_2^{600} for all residues is 140 ± 20 ms with an average error of 1 ms. Excluding those residues with NOE < 0.49 at 300 MHz, NOE < 0.6 at 500 MHz, and NOE < 0.65 at 600 MHz gives T_2^{600}/T_2^{300}, T_2^{500}/T_2^{300}, and T_2^{600}/T_2^{500} ratios of 0.9 ± 0.1, 1.0 ± 0.1, and 0.96 ± 0.09, respectively. The pattern of T_2 values is similar for all three fields. The average NOE^{300} for all residues is 0.55 ± 0.11 with an average error of 0.06, the average NOE^{500} for all residues is 0.65 ± 0.11 with an average error of 0.01, and the average NOE^{600} for all residues is 0.73 ± 0.10 with an average error of 0.01 (Figure 1c). The average NOE^{600}/NOE^{300}, NOE^{500}/NOE^{300}, and NOE^{600}/NOE^{500} ratios excluding those residues with NOE^{300} < 0.49, NOE^{500} < 0.60, and NOE^{600} < 0.65 are 1.2 ± 0.2, 1.2 ± 0.2, and 1.03 ± 0.08. The average T_1^{600}/T_2^{600}, T_1^{500}/T_2^{500}, and T_1^{300}/T_2^{300} ratios were 4.1 ± 0.3, 3.2 ± 0.2, and 1.8 ± 0.3, using residues not affected by internal motions.

For Ca^{2+}-cNTnC, relaxation data were collected at 500 MHz and chemical shift assignments were checked using the 3D HNHA experiment. The average T_1 was 440 ± 106 ms with an average error of 12 ms for 71 of 89 residues (Figure 3a). The average T_2 for all characterized residues was 166 ± 82 ms with an average error of 5 ms (Figure 3b). The average NOE was 0.57 ± 0.27 with an average error of 0.04 (Figure 3c). The average NOE value for Ca^{2+}-cNTnC is somewhat lower than expected from theory (NOE maximum is 0.76 for τ_m = 5.02 ns, S^2 = 0.85, and τ_e = 0 ps). We feel that this may be related to spectrometer drift, given the long acquisition times required to collect spectra with and without NOE (∼46 h/spectrum); also the spectrum with NOE was acquired after the spectrum without NOE. Thus, residues with an NOE < 0.566 were selected as those with significant internal motions and are 3, 4, 5, 12, 29, 32, 37, 51, 57, 64, 66, 84, 85, 86, 88, and 89. These residues are in the N and C termini, and the defunct Ca^{2+}-binding site. Excluding these residues, the average T_1/T_2 ratio is 2.8 ± 0.3.

Determination of the Overall Correlation Time. Backbone amide ^{15}N NMR relaxation data in proteins are often interpreted with the Lipari-Szabo model-independent formalism. In this approach, it is common to assume that the overall rotational tumbling of the protein is isotropic, and the correlation time (τ_m) associated with the overall rotation usually dominates the relaxation data. Internal flexibility is accounted for by adjusting the values of S^2 and the internal correlation time (τ_e). For apo-cNTnC, relaxation data acquired at 300, 500, and 600 MHz were treated separately. The τ_m was determined with the assumption that the rotational tumbling of the molecule is isotropic. The average values of the principal axes of the inertia tensor are 1.00:0.91:0.76 using residues 1−89 of the ensemble of forty solution structures, indicating that rotational tumbling is isotropic to a first approximation. The overall correlation time was determined from the average obtained from per residue fits of the relaxation data to the S^2-τ_m-τ_e model (isotropic rotational tumbling), and using only relaxation data for residues with NOE^{300} > 0.49, NOE^{500} > 0.60, and NOE^{600} > 0.65, as previously described (*32*). The correlation time for apo-cNTnC was determined to be 5.48, 5.53, and 5.55 ns based on 300, 500, and 600 MHz relaxation parameters, respectively.

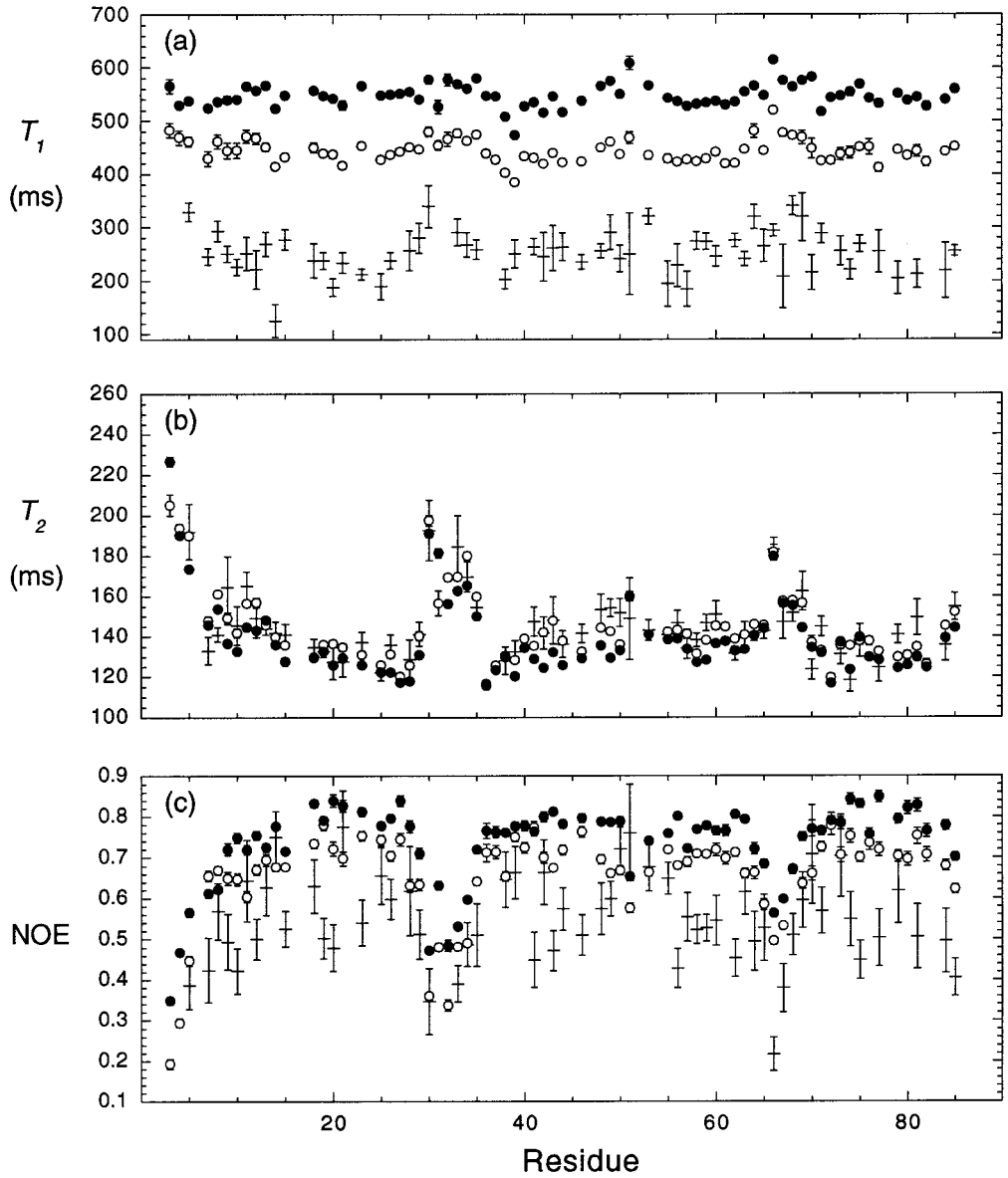

FIGURE 1: Plots of ^{15}N-T_1 (a), ^{15}N-T_2 (b), and {^{1}H}^{15}N NOE (c) at 300 (+), 500 (○), and 600 (●) MHz for apo-cNTnC. The elements of secondary structure are N helix (5−11), A helix (14−26), B helix (38−48), C helix (54−64), D helix (74−84), β strand (35−37,71−73), site 1 (28−40), site 2 (65−76), and the BC linker (49−53). Note that T_1 and T_2 increase with increasing internal motion. For example, the N-terminal residues and sites 1 and 2 show significantly larger T_1 and T_2 values compared to surrounding regions of secondary structure. The NOE is expected to decrease with increasing internal flexibility, and the N-terminal residues and sites 1 and 2 show significantly decreased NOEs compared to surrounding regions of secondary structure. Excluding flexible residues, the average T_1^{600}/T_1^{300}, T_1^{500}/T_1^{300}, and T_1^{600}/T_1^{500} ratios of 2.2 ± 0.4, 1.8 ± 0.3, and 1.25 ± 0.07, respectively, are close to the theoretical ratios of 2.16, 1.74, and 1.24 for a τ_m of 5.52 ns with $S^2 = 0.85$ (see Results). The average T_2^{600}/T_2^{300}, T_2^{500}/T_2^{300}, and T_2^{600}/T_2^{500} ratios of 0.9 ± 0.1, 1.0 ± 0.1, and 0.96 ± 0.09, respectively, are comparable to the theoretical ratios of 0.99, 1.03, and 0.97 (see Results). The average NOE^{600}/NOE^{300}, NOE^{500}/NOE^{300}, and NOE^{600}/NOE^{500} ratios of 1.2 ± 0.2, 1.2 ± 0.2, and 1.03 ± 0.08, which exclude flexible residues, are close to the theoretical ratios of 1.27, 1.22, and 1.04. Detailed analyses of the relaxation data (rotational diffusion anisotropy (Table 1) and entropic changes (Table 2)) utilized only 500 and 600 MHz relaxation data because these data sets contained more residues and were of higher quality than the 300 MHz relaxation data.

Recently, it has been shown that a small degree of anisotropy in the rotational tumbling of a protein can be reflected in the relaxation data (*32, 40*−*42*). Using an approach similar to that for apo-sNTnC (*32*), the $D_\parallel/D_\perp$ ratio for an axially symmetric diffusion tensor was determined to be 1.12 from an analysis of the T_1/T_2 ratios at 500 and 600 MHz for residues in the α helices of apo-cNTnC (Table 1), indicating that the degree of anisotropy in the rotational tumbling of apo-cNTnC is small. Relaxation data at 300 MHz were not used in the analysis of rotational tumbling anisotropy because the 500 and 600 MHz relaxation data were of significantly superior quality. Values of $D_\parallel/D_\perp$ close to 1 will not affect the determination of S^2 and τ_m when assuming that the rotational tumbling is isotropic. The coordinates used for the calculation of the rotational diffusion anisotropy were from the ensemble of 40 solution NMR structures (*17*).

The τ_m for Ca^{2+}-cNTnC is dependent upon protein concentration. For example, at a protein concentration of about 0.37 mM, τ_m was determined to be 6 ns. This value is reduced to 5 ns at a protein concentration of 0.15 mM. The concentration dependence of τ_m may be due to Ca^{2+}-induced protein dimerization and solution viscosity effects due to the

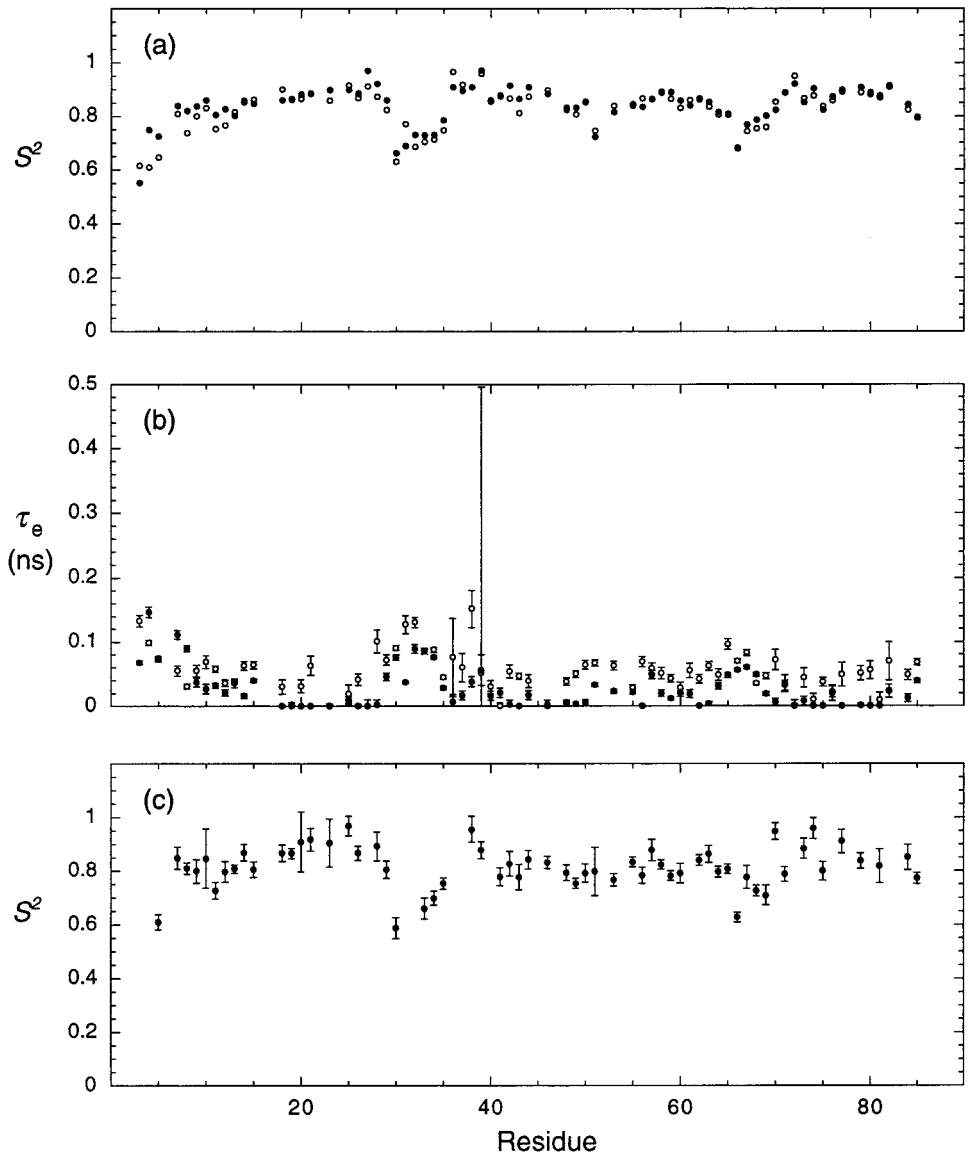

FIGURE 2: (a) Order parameters (S^2) and (b) internal correlation times (τ_e) for apo-cNTnC derived from the S^2-τ_m-τ_e model at 500 (○) and 600 (●) MHz and (c) S^2 for apo-cNTnC derived from the S^2-τ_m-τ_e model at 300 MHz. Elements of secondary structure are as in Figure 1. The error bars for S^2 at 500 and 600 MHz are smaller than the symbols used to indicate the values and are not shown. The average S^2 value for residues in well-defined regions of secondary structure is ~0.85 (*43*). Sites 1 and 2, residues in the N helix, and residue Asn-51 in the BC linker show S^2 values well below 0.85, indicating an increase in the amplitude of internal motion (greater flexibility) for these residues compared to the helices and β sheet. Values of τ_e are extremely sensitive to the measured NOE (*28*), and the systematically elevated NOE^{600} leads to smaller τ_e values at 600 MHz compared to 500 MHz (see Figure 1c).

dilution of the protein. The average values of the principal components of the inertia tensor were determined to be 1.00: 0.89:0.71 using residues 1−89 in the ensemble of 40 solution structures, justifying the assumption of isotropic rotational tumbling for the Ca^{2+}-saturated protein. In addition, the anisotropy of diffusion $D_\parallel/D_\perp$ for an axially symmetric diffusion tensor was determined to be 1.30 for Ca^{2+}-cNTnC (Table 1), using coordinates for the ensemble of 40 solution NMR structures (*17*). For a protein concentration of 0.15 mM, τ_m was determined from relaxation data with $NOE^{500} > 0.566$.

Model-Independent Analysis of Backbone Dynamics. One of the primary goals of this paper is to extract reliable values of S^2 for apo- and Ca^{2+}-saturated cNTnC in order to calculate the conformational entropy change for this two-state transition. The model-independent analysis for cNTnC was carried out under the assumption of isotropic rotational tumbling. For each residue, relaxation data were fitted to five spectral density models. These included an S^2-τ_m model, S^2-τ_m-τ_e, S^2-τ_m-R_{ex}, S^2-τ_m-τ_e-R_{ex}, and a two time scale model. S^2 values from the S^2-τ_m-τ_e model are usually reliable for the calculation of the conformational entropy changes associated with calcium binding, even in the presence of a small degree of rotational tumbling anisotropy. However, for some residues in sites 1 and 2, S^2 values from the S^2-τ_m-R_{ex} model were used due to significant improvements in the fit over the S^2-τ_m-τ_e model for apo- and Ca^{2+}-cNTnC (Table 2). In addition, the lower than expected average NOE for Ca^{2+}-cNTnC (see Results) has no effect on the determined τ_m and S^2 values but increases τ_e values. Thus, S^2 values will be reliable for the calculation of conformational entropy changes, even in the presence of systematic error for the NOE data, as previously noted (*32*).

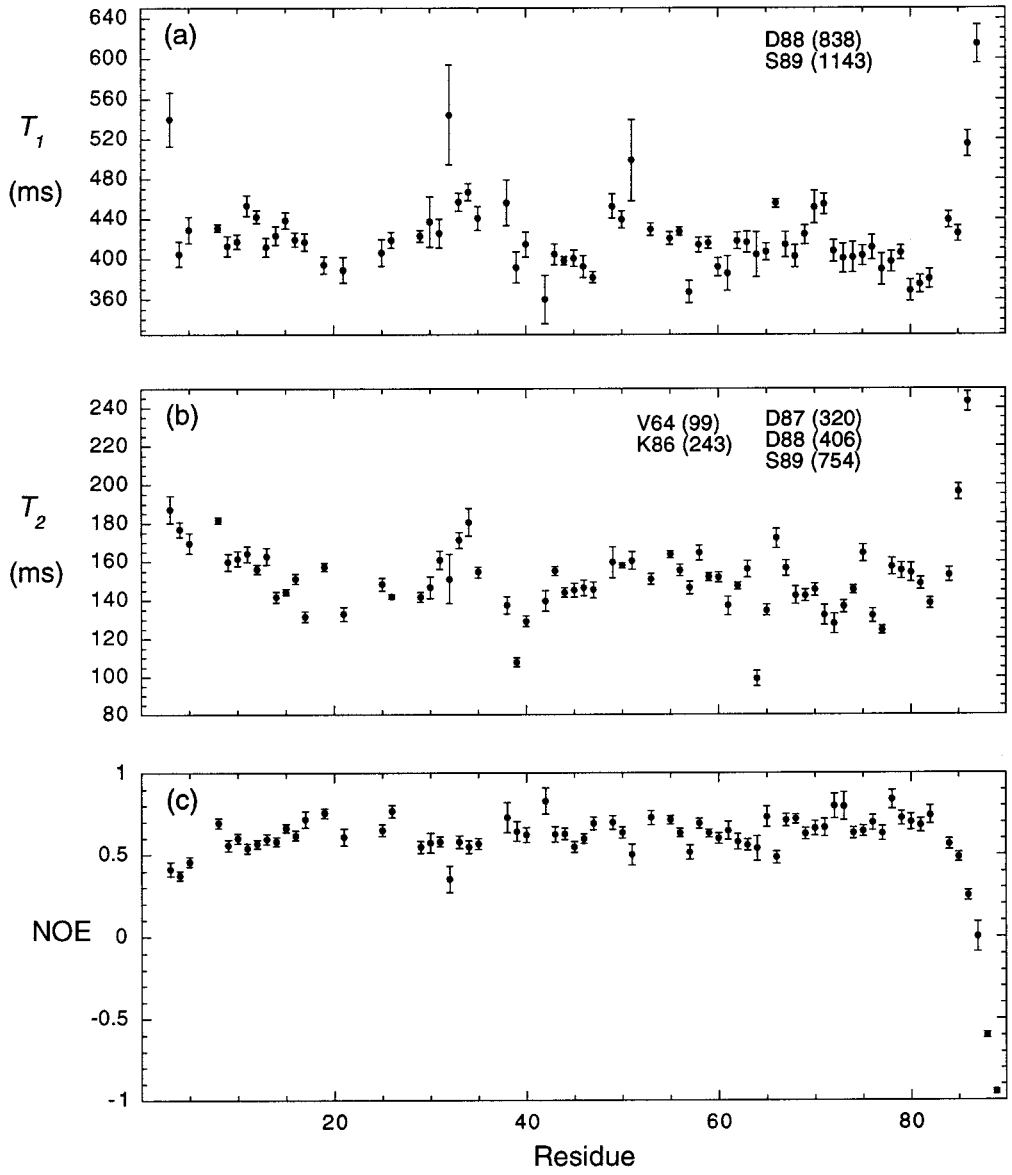

FIGURE 3: Plots of ^{15}N-T_1 (a), ^{15}N-T_2 (b), and {^{1}H}^{15}N NOE (c) at 500 MHz for Ca^{2+}-cNTnC. The elements of secondary structure are N helix (5−11), A helix (14−26), B helix (38−48), C helix (54−64), D helix (74−84), β strand (35−37,71−73), site 1 (28−40), site 2 (65−76), and the BC linker (49−53). The average T_1/T_2 value of 2.8 ± 0.3, excluding flexible residues, corresponds well with the theoretical value of 2.8 for a τ_m of 5.02 ns with $S^2 = 0.85$.

Table 1: Rotational Diffusion Anisotropy of cNTnC[a]

	apo (500 MHz)	apo (600 MHz)	Ca^{2+} (500 MHz)
θ	53 ± 7	55 ± 5	84 ± 8
ϕ	−18 ± 10	−32 ± 7	−19 ± 7
$D_\parallel/D_\perp$	1.13 ± 0.03	1.11 ± 0.02	1.30 ± 0.03
E	241 ± 23	322 ± 34	230 ± 18
E_v	6.5 ± 0.6	8.7 ± 0.9	7.4 ± 0.6
F_x	3.8 ± 1.5	5.7 ± 1.9	5.0 ± 1.2

[a] Values in the table are the averages and standard deviations from the ensembles of forty solution NMR structures for apo- and Ca^{2+}-cNTnC. θ, ϕ, $D_\parallel/D_\perp$, E, E_v, and F_x are as defined in Table 2 of ref *32*.

The average S^2 is 0.84 ± 0.06, 0.85 ± 0.05, and 0.86 ± 0.04 at 300, 500, and 600 MHz using residues with $NOE^{300} > 0.49$, $NOE^{500} > 0.60$, and $NOE^{600} > 0.65$ for apo-cNTnC, and the S^2-τ_m-τ_e model (Figure 2a). For Ca^{2+}-saturated cNTnC, the average S^2 was 0.86 ± 0.06 for residues with $NOE^{500} > 0.566$ and the S^2-τ_m-τ_e model (Figure 4a). The S^2 values indicate that for apo-cNTnC, the N-terminal residues, both Ca^{2+}-binding sites, and the BC interhelical region are flexible (Figure 2a). While the C-terminal residues are also expected to be flexible, dynamics data for these residues are not included due to spectral overlap. For Ca^{2+}-cNTnC, the S^2 values indicate that the N- and C-terminal residues, site 1, and the BC linker are flexible. Site 2 becomes more rigid upon Ca^{2+} binding, as well as defunct site 1 (Figures 4a and 7).

An analysis of rotational tumbling anisotropy requires high-quality relaxation data, and for apo-cNTnC, we did not use 300 MHz data, as the 500 and 600 MHz data contained more characterized residues and were of superior quality. Seven residues required an R_{ex} term to fit the T_2 data to within 95% confidence limits for apo-cNTnC at 500 and 600 MHz. Of these seven residues, five are in the A helix. As in the case of apo-sNTnC, this is due to the unique orientation of the A helix with respect to the principal axis of the rotational diffusion tensor, and not a conformational exchange phenomenon (*32*). On the other hand, the observed line broaden-

Table 2: Ca^{2+}-Induced Conformational Entropy Changes in Sites 1 and 2 of cNTnC

residue	S^2 apo[a]	S^2 Ca^{2+}	$-T\Delta S_p(j)$[b] (kcal/mol)	residue	S^2 apo[a]	S^2 Ca^{2+}	$-T\Delta S_p(j)$[b] (kcal/mol)
29	0.843 ± 0.007	0.844 ± 0.011	0.004 ± 0.053	65	0.808 ± 0.008	0.920 ± 0.014	0.56 ± 0.11
30	0.647 ± 0.009	0.840 ± 0.028	0.53 ± 0.11	66	0.681 ± 0.006	0.743 ± 0.009	0.15 ± 0.03
31	0.688 ± 0.008	0.796 ± 0.018	0.29 ± 0.06	67	0.757 ± 0.006	0.835 ± 0.016	0.25 ± 0.06
32	0.708 ± 0.011	0.736 ± 0.041	0.07 ± 0.11	68	0.771 ± 0.006	0.889 ± 0.021	0.47 ± 0.12
33	0.717 ± 0.009	0.752 ± 0.012	0.09 ± 0.04	69	0.780 ± 0.010	0.886 ± 0.016	0.42 ± 0.09
34	0.722 ± 0.007	0.732 ± 0.015	0.02 ± 0.04	70	0.831 ± 0.016[c]	0.797 ± 0.031[c]	−0.12 ± 0.12
35	0.767 ± 0.005	0.807 ± 0.014	0.13 ± 0.05	71	0.889 ± 0.006[c]	0.792 ± 0.019[c]	−0.40 ± 0.07
36	0.861 ± 0.014[c]	ND[d]		72	0.877 ± 0.014[c]	0.884 ± 0.026[c]	0.04 ± 0.16
37	0.874 ± 0.017[c]	0.803 ± 0.03[c]	−0.29 ± 0.13	73	0.860 ± 0.014	0.927 ± 0.02	0.41 ± 0.18
38	0.910 ± 0.007	0.894 ± 0.024	−0.10 ± 0.15	74	0.863 ± 0.014	0.873 ± 0.014	0.05 ± 0.10
39	0.965 ± 0.017[e]	0.919 ± 0.028[c]	−0.30 ± 0.30	75	0.831 ± 0.009	0.829 ± 0.016	−0.008 ± 0.069
40	0.858 ± 0.007	0.869 ± 0.025[c]	0.05 ± 0.13	76	0.866 ± 0.013	0.923 ± 0.017	0.35 ± 0.15
			0.5 ± 0.4				2.2 ± 0.4

[a] S^2 values for apo-cNTnC are the averages of the 500 and 600 MHz relaxation data. However, the ^{15}N-T_2 value for Ala-31 at 500 MHz was found to be biased and gives rise to a large S^2. Thus, the value of S^2 for Ala-31 is from the 600 MHz data. [b] Measurement uncertainties for S^2 were propagated in the standard manner (*56*). [c] S^2 values for these residues were taken from the S^2, R_{ex} model. [d] Not determined. [e] The value of S^2 for Lys-39 is at the upper limit ($S^2 \sim 0.95$) of the applicability of eq 1, where the classical description of conformational entropy breaks down (*30*), and the value for $-T\Delta S_p$ was calculated by assuming $S^2 = 0.95$ for this residue.

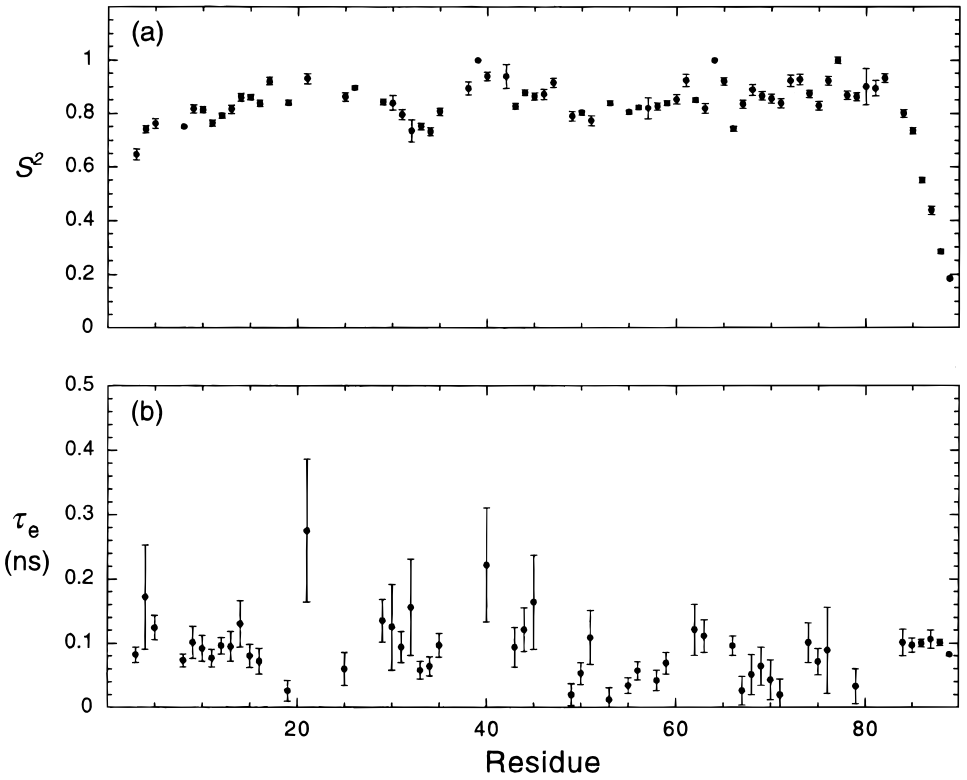

FIGURE 4: S^2 (a) and τ_e (b) for Ca^{2+}-cNTnC derived from the S^2-τ_m-τ_e model at 500 MHz. Elements of secondary structure are as in Figure 3. Residues Lys-39 at the beginning of the B helix, Val-64 at the hinge of the C helix, and Phe-77 in the D helix have significantly decreased T_2s; thus the S^2-τ_m-τ_e model is not appropriate and gives rise to unusually large order parameters ($S^2 = 1$) for these residues. Residues in the N helix, sites 1 and 2, and the C-terminus show larger amplitude internal motions ($S^2 < 0.85$) than expected for regions of well-defined secondary structure ($S^2 \sim 0.85$). Values of τ_e are not shown for residues in which the error in τ_e is significantly greater than the fitted value.

ing for some residues in sites 1 and 2 reflects a conformational exchange phenomenon, and not rotational tumbling anisotropy, as identified using the criteria of Tjandra and Bax (*40*). These include residues 36 and 72 for apo-cNTnC at 500 and 600 MHz. Nine residues required a two time scale model to fit the relaxation data for apo-cNTnC to within 95% confidence limits at 500 and 600 MHz. These include residues at the beginning of the N helix and the Ca^{2+}-binding loops. One residue was not fit by any model at 500 MHz, and six residues were not fit at 600 MHz.

For Ca^{2+}-cNTnC, 15 residues required an R_{ex} term to fit the relaxation data to within 95% confidence limits. Of these 15, four are in the A helix, three in the β sheet, four in site 1, one in site 2, one in the C helix, one in the D helix, and one in the BC linker. It should be noted, however, that, unlike apo-cNTnC, we do not have the benefit of an independent analysis at 600 MHz to further validate the inclusion of an R_{ex} term for a given residue due to the lack of an 8 mm triple resonance probe for our Unity 600 spectrometer. By using the criteria of Tjandra and Bax (*40*), residues 37−39

Table 3: Amino Acid Sequences of Sites 1 and 2 in c- and sNTnC[a]

E−F hand position		1	2	3	4	5	6	7	8	9	10	11	12
site 1	sNTnC	**D**	A	**D**	G	**G**	G	**D**	I	**S**	T	K	**E**
	cNTnC	**L**	G	**A**	E	**D**	G	**C**	I	**S**	T	K	**E**
site 2	sNTnC	**D**	E	**D**	G	**S**	G	**T**	I	**D**	F	E	**E**
	cNTnC	**D**	E	**D**	G	**S**	G	**T**	V	**D**	F	D	**E**

[a] Positions involved in coordinating Ca^{2+} in the E−F hand family of Ca^{2+}-binding proteins are indicated by bold underlined letters. The Asp side chains at positions 1 and 3 and the Glu side chain at position 12 in site 1 coordinate Ca^{2+} through their carboxyl oxygens (Glu at position 12 is a bidentate ligand whereas the Asp residues are monodentate). Position 7 contributes a ligand via the backbone carbonyl, and positions 5 and 9 coordinate Ca^{2+} through water molecules. Site 2 coordinates Ca^{2+} in a fashion similar to that of site 1, with the exception that the Ser at position 5 coordinates Ca^{2+} through its side chain hydroxyl oxygen and not water (*44*).

and 71 were identified as residues undergoing conformational exchange phenomena. Eight residues required a two time scale model to fit the relaxation data to within 95% confidence limits. These residues included two in the N helix, two at the end of the D helix, one at the beginning of the D helix, one at the end of the B helix, and two in the C helix. As in the case of the R_{ex} term, we do not have the benefit of an independent data set at 600 MHz to further justify the use of the two time scale model. Seven residues were not fit by any model for Ca^{2+}-cNTnC at 500 MHz.

DISCUSSION

The dynamics data presented here show, for the first time, the Ca^{2+}-induced changes in the backbone dynamics and thermodynamics in cNTnC as determined by ^{15}N NMR relaxation measurements. The apo- and Ca^{2+}-saturated solution structures of cNTnC reveal that the N, A, and D helices form a structural unit which remains invariant to Ca^{2+} binding, and that the B and C helices move slightly away from the NAD unit upon Ca^{2+} binding (*17*). The interhelical reorientations that occur upon Ca^{2+} binding are reflected in the relaxation data as a difference in the rotational diffusion anisotropy of the apo- and Ca^{2+}-saturated states, as Ca^{2+}-cNTnC is somewhat less compact than apo-cNTnC. The differences in flexibility between sites 1 and 2 in apo-sNTnC show that site 2 is more rigid than site 1 by about 1 kcal mol^{-1} (*32*). In contrast, sites 1 and 2 in apo-cNTnC are similar in flexibility; this is due in part to site 1 sequence differences in cNTnC compared to sNTnC which abolish Ca^{2+} binding in this site (Table 3). The entropic difference between sites 1 and 2 in apo-cNTnC determined from changes in picosecond to nanosecond time scale fluctuations is small, with a value of 0.3 ± 0.3 kcal mol^{-1}. Upon Ca^{2+} binding to site 2, residues within the flexible loops of the binding site (positions 2−6 of 12 positions) become more rigid as some of the side chains of the loop residues take up specific conformations in order to ligate Ca^{2+}. Suprisingly, flexible loop residues within site 1 within cNTnC also become more rigid upon Ca^{2+} binding to site 2. The data show that sites 1 and 2 are structurally and thermodynamically coupled.

Rotational Correlation Time and Rotational Diffusion Anisotropy. The rotational correlation times for apo-cNTnC were determined to be 5.48 ± 0.12, 5.53 ± 0.11, and 5.55 ± 0.10 ns using 300, 500, and 600 MHz relaxation data, respectively, at 30 °C and with the sample conditions described in the Methods. These correlation times are the averages obtained from per residue fits of the relaxation data to the S^2-τ_m-τ_e model, excluding residues with $NOE^{300} > 0.49$, $NOE^{500} > 0.60$, and $NOE^{600} > 0.65$. The agreement between the three fields for τ_m is excellent, and the average is 5.52 ± 0.06 ns. This correlation time is somewhat longer than that found for apo-sNTnC at 30 °C (4.86 ± 0.15 ns). However, it should be noted that the solvent composition differs for the two isoforms. Specifically, apo-cNTnC contains 15 mM DTT which may increase the solution viscosity compared to apo-sNTnC. Additionally, apo-cNTnC may be slightly aggregated, which could give rise to an increased correlation time. While aggregated proteins show unusually large correlation times and increased S^2 values, the average S^2 value for apo-cNTnC excluding flexible residues is 0.85, which corresponds well to the S^2 value expected for regions of well-defined secondary structure in proteins (*43*). Thus, if aggregation is present for apo-cNTnC, it does not appear to affect the S^2 values significantly. The correlation time determined for Ca^{2+}-cNTnC is 5.02 ± 0.22 ns at 30 °C and is the average obtained from per residue fits of the relaxation data to the S^2-τ_m-τ_e model, excluding residues with NOE > 0.566. This correlation time is shorter than that for apo-cNTnC, perhaps due to the aggregation of apo-cNTnC, or it may be due to solution viscosity effects upon dilution of Ca^{2+}-cNTnC and the presence of Ca^{2+} in the sample.

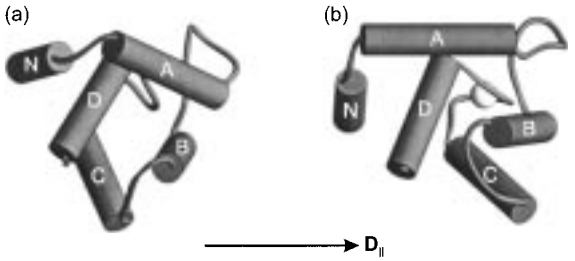

FIGURE 5: Minimized average NMR solution structures of apo (a) and Ca^{2+}-saturated (b) cNTnC (*17*) oriented with respect to the long axis of the rotational diffusion tensor ($D_{||}$) which lies along the plane of the page. Ca^{2+}-cNTnC is more elongated along $D_{||}$, accounting for the larger $D_{||}/D_{\perp}$ ratio compared to apo-cNTnC.

For apo-cNTnC, the average $D_{||}/D_{\perp}$ ratio (1.12) determined from 500 and 600 MHz relaxation parameters for an axially symmetric anisotropic rotational diffusion tensor is comparable to the value of 1.10 for apo-sNTnC, indicating that the rotational tumbling of both isoforms in the apo states is essentially isotropic. It should be noted that the probabilities that the improvement in the fits arose by chance when using an anisotropic rotational diffusion model are 0.019 and 0.0028 at 500 and 600 MHz, respectively. As noted previously (*32*), such a small degree of anisotropy in the tumbling of apo-cNTnC has little effect on S^2 when assuming the tumbling is isotropic. However, the R_{ex} terms required to fit

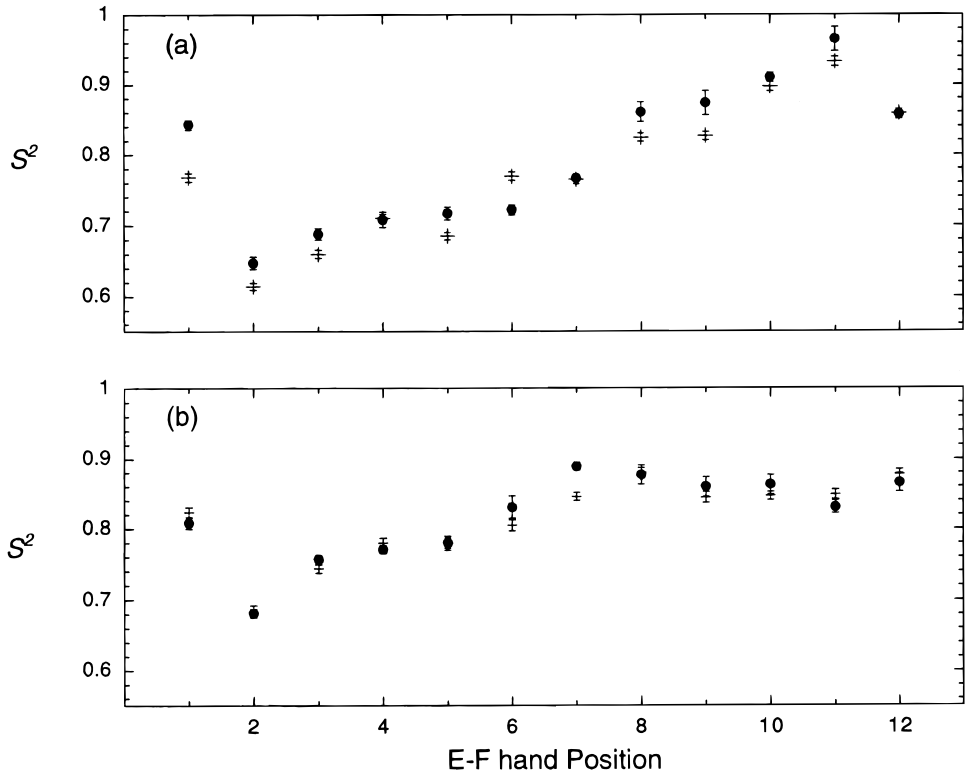

FIGURE 6: Comparison of S^2 for site 1 (a) and site 2 (b) in apo-sNTnC (+) and apo-cNTnC (●). The averages of the 500 and 600 MHz data have been used for both isoforms. S^2 values for site 2 are similar for sNTnC and cNTnC, indicating that the flexibility of site 2 is similar in the two isoforms of NTnC. The first three positions of site 1 in apo-cNTnC are more rigid than their counterparts in sNTnC on account of hydrophobic interactions arising from the D29L, D31A sequence differences and the Val-28 insertion in cNTnC compared to sNTnC (see text).

the relaxation data for certain residues in the A helix are due to its unique orientation with respect to the long axis of the rotational diffusion tensor in comparison to helices N, B, C, and D (Figure 5).

For Ca^{2+}-cNTnC, the relaxation data are more adequately described by axially symmetric anisotropic diffusion with a $D_{\parallel}/D_{\perp}$ ratio of 1.30. The structure of apo-cNTnC is slightly more spherical and compact than Ca^{2+}-cNTnC with respect to the long axis of the rotational diffusion tensor. The probability that the improvement in the fit for anisotropic above isotropic rotational tumbling arose by chance is 0.0067, justifying the use of an axially symmetric anisotropic rotational tumbling model. The larger anisotropy for the rotational diffusion tensor of Ca^{2+}-cNTnC is not surprising, given the different orientations of the B and C helices with respect to the N, A, and D helices compared to apo-cNTnC (*17*) (Figure 5). It should be noted that the N, A, and D helices are structurally invariant to Ca^{2+} binding (*17*). As in the case of apo-cNTnC, the A helix adopts a unique orientation with respect to the long axis of the anisotropic rotational diffusion tensor, and therefore, the R_{ex} terms required to fit the relaxation data for five residues in this helix are due to anisotropic tumbling. Figure 5 shows the minimized average structures of apo- and Ca^{2+}-saturated cNTnC oriented with respect to the long axis of the rotational diffusion tensor.

Relevance of Backbone Amide Dynamics to Solution Structures. The ensemble of solution structures for apo-cNTnC shows regions of disorder (larger than average backbone RMSD) at the N and C termini, sites 1 and 2, and the BC linker (*17*). The backbone amide S^2 values show that sites 1 and 2 are more flexible on the picosecond to nanosecond time scale, as well as the BC linker, compared to regions of well-defined secondary structure. Interestingly, although the N helix is well-defined in the ensemble of solution structures, the relaxation data show that it is more flexible than helices A, B, C, and D (Figure 2a). This is likely due to the fact that it is a terminal helix that is not as highly packed as helices A, B, C, and D that pack against each other and contribute to the main hydrophobic core of apo-cNTnC. The ensemble of solution structures for Ca^{2+}-cNTnC reveals disordered regions at the N and C termini and sites 1 and 2 (*17*). Although the backbone RMSDs are larger for sites 1 and 2 compared to the well-defined regions, they are not as large as those for sites 1 and 2 in apo-cNTnC. The S^2 values indicate that the flexible loop region of site 2 (positions 2−6 of the 12 residue site) becomes significantly less flexible upon Ca^{2+} binding. For example, the average S^2 of 0.76 ± 0.05 for the flexible loop of site 2 in the apo state (using 500 and 600 MHz data) increases to 0.83 ± 0.06 in the Ca^{2+}-saturated state. The flexible loop region of site 1 also becomes more rigid compared to the apo state, with an average S^2 value for positions 2−6 of 0.70 ± 0.03 that increases to 0.77 ± 0.04 (Figure 4a and Table 2). The N helix is also more flexible than the other helices, as observed for apo-sNTnC.

Comparison of Site 1 and Site 2 Dynamics in apo-cNTnC. Sites 1 and 2 are coupled via the antiparallel β sheet in c- and sNTnC. The twelve residue E−F hand sites in apo-cNTnC are rigid at one end (positions 10−12) and become progressively more flexible at the opposite end (positions 2−4, Figures 6 and 7). A comparison of the crystal structures

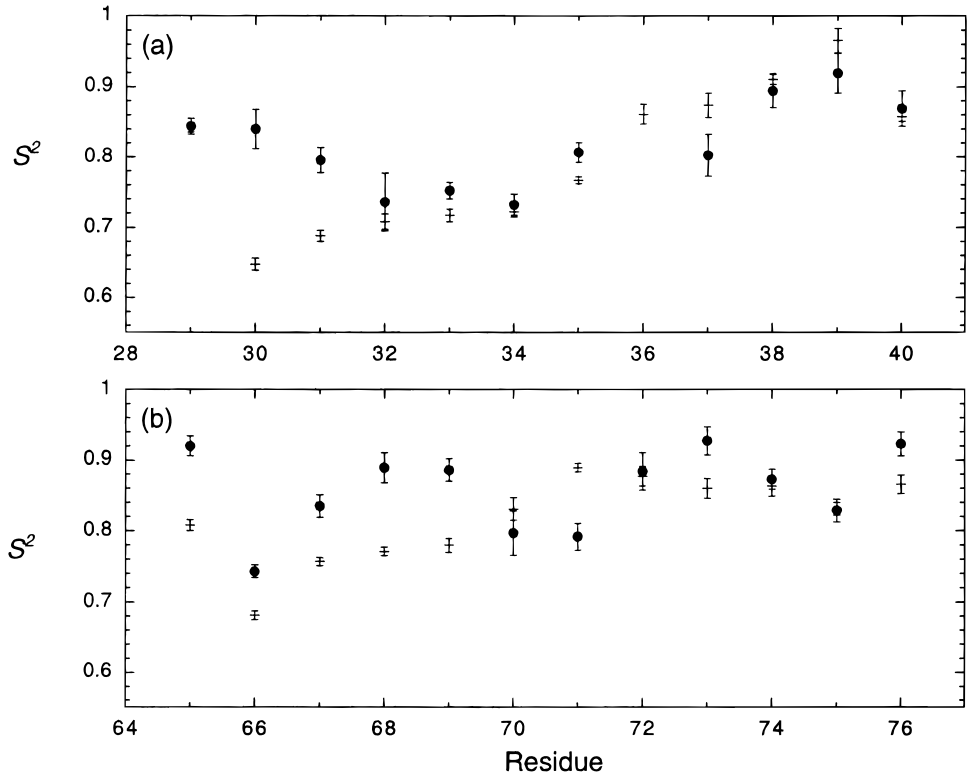

FIGURE 7: Comparison of S^2 for site 1 (a) and site 2 (b) in apo-cNTnC (+) and Ca^{2+}-cNTnC (●). The averages of the 500 and 600 MHz data have been used for apo-cNTnC. The first five positions in site 2 of cNTnC become more rigid upon binding Ca^{2+}. Positions 1, 3, and 5 of site 2 coordinate Ca^{2+} via side chain carbonyls (Table 3).

of helix-loop-helix calcium-binding proteins led to the suggestion that the carboxylate side chain at position 1 hydrogen bonds with the backbone amide proton at position 6 in the Ca^{2+}-saturated state (*44*), and that this interaction is also important in stabilizing site 2 in the apo state for sNTnC (*15*). The S^2 values for Asp-65 and Gly-70 in apo-cNTnC are 0.81 and 0.83, respectively. At the end of the β sheet closest to Gly-70, residues 37 and 71 are rigid, and they help stabilize Gly-70, supporting the suggestion that positions 1 and 6 are involved in a hydrogen-bonding interaction which is important in stabilizing site 2 in the apo state. In the ensemble of forty NMR solution structures for apo-cNTnC, the hydrogen bond between the amide proton of Gly-70 and the carboxylate oxygens (either $O^{\delta 1}$ or $O^{\delta 2}$) of Asp-65 has an occupancy of 60% with an average distance (HN−O) of 3.1 ± 0.3 Å (*17*) (see Figure 8). In comparison, the Asp to Leu mutation in position 1 of site 1 of cNTnC (Table 3) removes the hydrogen bond between positions 1 and 6 which stabilizes site 2 in the apo state. From the dynamics data presented here, the hydrogen bond formed between the side chain of Asp-65 and the main chain amide of Gly-70 is a more important factor in determining the Ca^{2+}-binding affinity of site 2 in cNTnC than proposed hydrogen bonds involving the backbone amides of positions 5 and 6 and the carboxlyate side chain of position 3 in sNTnC due to the greater flexibility at these residues (Asp-67, $S^2 = 0.76$; Ser-69, $S^2 = 0.78$) (*15*).

Another interesting difference between the Ca^{2+}-binding sites in apo-cNTnC is the fact that positions 10 and 11 (residues Thr-38 and Lys-39, respectively) are the most rigid residues of sites 1 and 2 in the apo state and are stabilized by interactions between the side chain methyl of Thr-38 and the side chain of Val-72, and hydrogen bonds between Ser-37 side chain and main chain oxygens with the backbone amide proton of Lys-39 (*15*, *17*). In the ensemble of forty NMR structures for apo-cNTnC, the hydrogen bond between the amide proton of Lys-39 and the O^{γ} of Ser-37 has 25% occupancy and an average HN−O^{γ} distance of 3.2 ± 0.2 Å, and the hydrogen bond between the amide of Lys-39 and the backbone carbonyl of Ser-37 has 33% occupancy and an average N−O distance of 2.7 ± 0.3 Å (*17*).

The Ca^{2+}-binding sites are coupled via the antiparallel β sheet in cNTnC, and there are differences in dynamics of the individual strands which each site contributes to the sheet. Residue Asp-73 for the β strand in site 2 (residues 71−73) is more rigid ($S^2 = 0.86$) than its partner (Cys-35, $S^2 = 0.77$) for the β strand in site 1 (residues 35−37), with Cys-35 being the most flexible in the β sheet. The central pair of residues in the β sheet (Ile-36 and Val-72) is connected by two hydrogen bonds: one between the backbone carbonyl of Ile-36 and the backbone amide proton of Val-72 which shows 100% occupancy in the ensemble of forty solution NMR structures and an average O−HN distance of 2.3 ± 0.1 Å, and another between the backbone carbonyl of Val-72 and the backbone amide proton of Ile-36 which shows 100% occupancy and an average O−HN distance of 2.1 ± 0.2 Å (*17*). One end of the β sheet is stabilized by a hydrogen bond between the backbone carbonyl of Gly-70 and the amide proton of Thr-38 (100% occupancy; average O−HN distance, 2.1 ± 0.3 Å), while at the other end, the hydrogen bond between the backbone carbonyl of Gly-34 and the amide proton of Phe-74 is weaker (20% occupancy; average O−HN distance, 3.2 ± 0.1 Å) and accounts, in part, for the greater flexibility observed for Cys-35 (see Figure 9).

Comparison to Site 1 and Site 2 Dynamics and Thermodynamics in apo-sNTnC. Following the work of Akke et al.

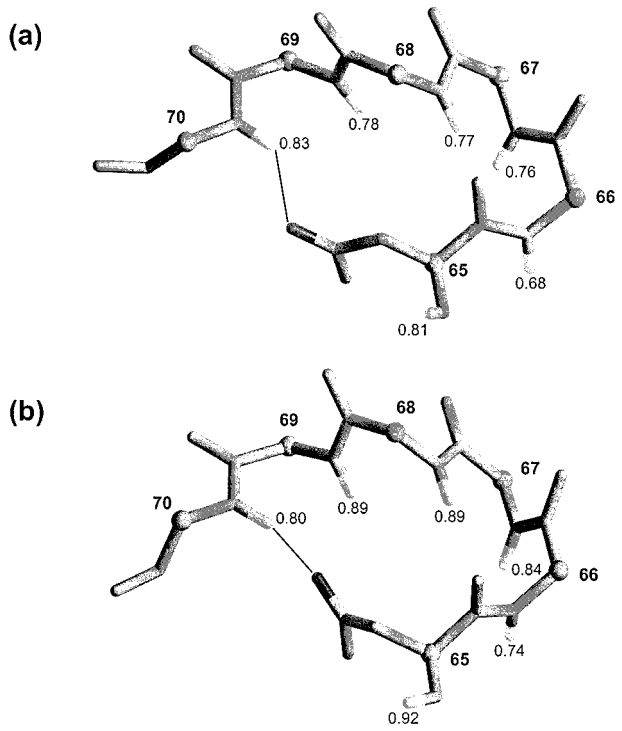

FIGURE 8: Backbone atoms (C^{α}, C, O, N, HN) for site 2 in apo- (a) and Ca^{2+}-cNTnC (b). The non-hydrogen side chain atoms for Asp-65 are also shown. S^2 values for the backbone amide nitrogens are indicated. The hydrogen bond between the backbone amide proton of Gly-70 and the carboxylate oxygen of Asp-65 is indicated by a line. This hydrogen bond is an important determinant of Ca^{2+} affinity in site 2 (see text). The figure was made with the program Ribbons (*57*).

(*29*), Daiwen Yang and Lewis E. Kay (*30*) developed methodology by which the change in conformational entropy associated with changes in picosecond to nanosecond bond vector fluctuations upon a two-state transition may be evaluated:

$$\frac{\Delta S_p(j)}{k} = \ln\left(\frac{3 - \sqrt{1 + 8S_b}}{3 - \sqrt{1 + 8S_a}}\right) \quad (1)$$

where k is Boltzmann's constant, $\Delta S_p(j)$ is the entropy change associated with the j^{th} backbone amide N−NH vector, S_a is the square root of the Lipari-Szabo order parameter for state a, and S_b is the square root of the Lipari-Szabo order parameter for state b. Equation 1 was used to calculate the entropic difference between sites 1 and 2 of apo-cNTnC and apo-sNTnC. As pointed out by Zuiderweg and co-workers, there are limitations to using only backbone amide ^{15}N relaxation data to characterize peptide plane motions (*45*). In addition, a more detailed characterization of dynamics is possible via side chain dynamics measurements (*46*, *47*).

The site 2 amino acid sequence in c- and sNTnC is highly conserved, whereas site 1 is sufficiently mutated in cNTnC to abolish Ca^{2+} binding entirely (Table 3 and Figure 6). Recently, the dynamics and thermodynamics of apo-sNTnC were evaluated using ^{15}N NMR relaxation measurements (*32*). Figure 6 shows that S^2 values for site 2 in apo-sNTnC and apo-cNTnC are similar, whereas for site 1, positions 1−3 are more rigid for apo-cNTnC compared to apo-sNTnC. A comparison of site 1 and site 2 thermodynamics of apo-sNTnC and apo-cNTnC reveals a decrease in conformational

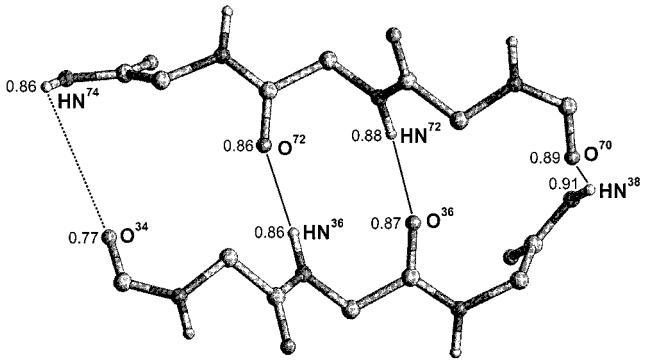

FIGURE 9: Backbone atoms (C^{α}, C, O, N, HN) of the central β sheet in apo-cNTnC. Strong hydrogen bonds are indicated by solid lines and weaker hydrogen bonds by dashed lines. The two central hydrogen bonds between the backbone amide protons and carbonyl oxygens of Ile-36 and Val-72 form the pivot point for the Ca^{2+}-induced transition in cNTnC. S^2 values across hydrogen-bonded pairs are indicated; note that, for the carbonyl oxygens, the S^2 values are from the backbone amide nitrogen of the following residue (i + 1) within the same peptide plane. The S^2 values across the central hydrogen bonds are well-matched. The figure was made with the program Ribbons (*57*).

entropy for site 1 of -0.9 ± 0.3 kcal mol^{-1} and no significant difference for site 2 of apo-cNTnC compared to the skeletal isoform. The conformational entropy differences were calculated using all residues in sites 1 and 2 for both isoforms of NTnC. Positions 1−3 of site 1 in apo-cNTnC contribute 0.37 ± 0.04 kcal mol^{-1} to a total decrease of 0.9 ± 0.3 kcal mol^{-1} in conformational entropy for this site compared to apo-sNTnC. Site 1 in cNTnC contains an insertion (Val-28) and might be expected to be more flexible than site 1 in sNTnC due to an increase in loop length. However, Val-28 and Leu-29 at the end of the A helix serve to stabilize position 1 of site 1 in apo-cNTnC compared to site 1 in apo-sNTnC. Val-28 and Leu-29 show S^2 values of 0.83 and 0.84, respectively, indicating that these residues are not flexible on the picosecond to nanosecond time scale. Val-28 is also highly packed, exposing only 20 ± 7 Å^2 of side chain accessible surface area, and makes several hydrophobic contacts to residues at position 3 (Ala-31) and positions 6−8 (Gly-34, Cys-35, and Ile-36) of site 1 (*17*). In addition, there is a hydrogen bond between the main chain carbonyl of Val-28 and main chain amide proton of Gly-30 in the apo state which has an occupancy of 25% and an average O−HN distance of 2.6 ± 0.1 Å (*17*). Leu-29 makes hydrophobic contacts to Ile-36 and Ser-37 within the β sheet of site 1. The Gly-Gly-Gly sequence at positions 4−6 in site 1 of sNTnC is not appreciably more flexible compared to the Glu-Asp-Gly sequence in cNTnC (Figure 6). In fact, the flexible binding loops of site 1 in apo-cNTnC and apo-sNTnC are similar in flexibility, each with an average S^2 of 0.76 ± 0.05.

The results give insight into the binding affinities for site 2 in c- and sNTnC. For sNTnC, the mutation of a single ligand at position 12 of site 1 (E41A) diminishes the calcium affinity of this site significantly and concomitantly causes a 10-fold reduction in the Ca^{2+} affinity for site 2 (*22*). In contrast, although cNTnC has an inactive site 1, site 2 has a binding affinity similar to that for site 2 in native sNTnC. We attribute this difference between sNTnC and cNTnC in part to the "stiffer" site 1 in cNTnC.

Ca^{2+}-Induced Changes in Dynamics and Thermodynamics. Picosecond and nanosecond time scale fluctuations of the

backbone amide nitrogens in the Ca^{2+}-binding sites of cNTnC contribute $+2.7 \pm 0.6$ kcal mol^{-1} to the free energy of Ca^{2+} binding to site 2. As shown in Table 2, there is a decrease in conformational entropy in the Ca^{2+}-binding loops of both sites 1 and 2 (residues 30−34, and 66−70, respectively, i.e., positions 2−6 of the 12 residue sites) upon Ca^{2+} binding. Ca^{2+} binding to site 2 in cNTnC leads to a significant increase in S^2 for the flexible loop residues, as observed for Ca^{2+} binding to the archetypal site 2 in calbindin D_{9k} (*48*). In the apo state, positions 2−6 in site 2 of cNTnC show S^2 values of 0.68, 0.76, 0.77, 0.78, and 0.83, and these values change to 0.74, 0.84, 0.89, 0.89, and 0.80 upon Ca^{2+} binding, as shown in Figure 7. In the apo state, positions 2−6 in site 1 show S^2 values of 0.65, 0.69, 0.71, 0.72, and 0.72 that increase to 0.84, 0.80, 0.74, 0.75, and 0.73 upon Ca^{2+} binding (Figure 7). The changes in the binding loops account for $+1.0 \pm 0.2$ and $+1.2 \pm 0.2$ kcal mol^{-1} from sites 1 and 2, respectively, of the conformational entropy contribution to the free energy of Ca^{2+} binding to site 2 of cNTnC. These results are consistent with the initial observation that the dominant contribution to the free energy of cooperative Ca^{2+} binding to sites 1 and 2 in calbindin D_{9k} arises from the stiffening of backbone residues within the flexible loop of the Ca^{2+}-binding site 2 (*29*). Within the β sheet, the paired residues, Ser-37 and Thr-71, become more flexible upon Ca^{2+} binding. Residues Cys-35 and Val-72 at the other end of the β sheet, on the other hand, become more rigid compared to the apo state. Thus, entropic changes at one end of the β sheet cancel those at the other end (Ser-37/Thr-71 -0.7 ± 0.2 kcal mol^{-1}; Cys-35/Asp-73 $+0.5 \pm 0.2$ kcal mol^{-1}) upon Ca^{2+} binding. Interestingly, a hydrogen bond between the amide proton of Thr-39 and the carbonyl oxygen of Gly-71 is broken upon Ca^{2+} binding to sites 1 and 2 in sNTnC (*15*). In the ensemble of NMR solution structures for Ca^{2+}-cNTnC, this hydrogen bond shows an occupancy of 20% and an average O−HN distance of 3.0 ± 0.2 Å compared to 100% occupancy and an average distance of 2.1 ± 0.3 Å in the apo state, for the analogous residues Thr-38 and Gly-70 (*17*). The loss of this hydrogen bond is consistent with the greater flexibility observed at this end of the β sheet (Ser-37/Thr-71) in Ca^{2+}-cNTnC compared to the apo state.

For the central pair of residues in the β sheet, relaxation data are available only for Val-72, and the S^2 values in the apo and Ca^{2+} states are similar, indicating that there is no change in flexibility for Val-72 upon Ca^{2+} binding. The changes in S^2 for the β sheet upon Ca^{2+} binding suggest that the pivot point for the Ca^{2+}-induced transition in cNTnC occurs at residues Ile-36 and Val-72 in the β sheet, and that, while the β sheet was more flexible at Cys-35 in the apo state, it becomes more flexible at the opposite end (residues Ser-37 and Thr-71) upon Ca^{2+} binding. While relaxation data is not available for Ile-36 in the Ca^{2+}-saturated state, we can estimate that the total entropic change for site 1 does not change if we assume that the changes in S^2 for Ile-36 upon Ca^{2+} binding are similar to those for Val-72 (Table 2).

The stiffening of the β sheet at Cys-35 is a consequence of stabilizing hydrophobic interactions between Cys-35 and Val-28/Ala-31. This mechanism is an important factor in the coupling of the two Ca^{2+}-binding sites and allows for the stiffening of positions 1−3 in site 1 when Ca^{2+} binds in site 2.

Another notable change upon Ca^{2+} binding is that position 12 in site 2 becomes significantly more rigid in the Ca^{2+}-saturated state. Glu-76 in site 2 coordinates Ca^{2+} via its bidentate side chain and is therefore expected to be more rigid in the Ca^{2+} state.

Interestingly, position 2 in the active Ca^{2+}-binding site 2 is observed to be flexible in the Ca^{2+}-saturated state. This is somewhat surprising considering that the side chains of residues at positions 1 and 3 are involved in Ca^{2+} ligation. However, as pointed out by Baldellon et al., position 2 in the second site of Ca^{2+}-saturated parvalbumin and the corresponding residue in the C-terminal domain of Ca^{2+}-saturated calmodulin are also flexible for these paired E−F hand proteins (*49*). It has been proposed that position 2 in the second E−F hand site is a flexible hinge between the helix at the N-terminal end of the Ca^{2+}-binding site and the remainder of the site (*49*).

CONCLUSIONS

Site−site interactions allow for the "stiffening" of site 1 when Ca^{2+} binds site 2 in cNTnC. In general, the Ca^{2+} affinity of a paired E−F hand moiety will be determined by the entire domain structure. In particular, hydrophobic interactions between α helices and across β strands of paired Ca^{2+}-binding sites are major determinants of Ca^{2+} affinity, as demonstrated in several studies of homodimers and heterodimers of E−F hand peptides (*50*−*54*). The domain structure and sequences of apo-sNTnC and apo-cNTnC are similar (*17*). Thus, it is reasonable to assume that the principal reason site 2 maintains similar Ca^{2+} affinity in the two isoforms is the similarity of the domain structures. In addition to domain structure, the amino acid sequences of the sites play a key role in determining the Ca^{2+} affinity. For example, the single mutants E140Q of the C-terminal domain of calmodulin (*55*) and E41A-sNTnC (*20*) show drastically altered Ca^{2+} affinities in their mutated sites and structures compared to the native Ca^{2+}-saturated forms. For troponin C, the Ca^{2+} affinity of the sites in the regulatory domain is fine-tuned in part by their intrinsic conformational stability in the apo state, which is determined in part by intra- and inter-site interactions. For example, the recent demonstration that site 2 in apo-sNTnC is more rigid than site 1 (*32*) supports the suggestion that Ca^{2+} binds first to site 2 in sNTnC (*22*). For cNTnC, site 1 sequence differences compared to sNTnC that include an insertion (Val-28) and substitutions D29L and D31A allow hydrophobic interactions that stabilize site 1 in the apo- and Ca^{2+}-saturated states, and play a role in maintaining the Ca^{2+} affinity of site 2 similar to that in sNTnC.

ACKNOWLEDGMENT

We thank Drs. Murali Chandra and R. John Solaro for providing the cNTnC DNA construct; David Corson and Linda Saltibus for preparation of the cNTnC samples; Lewis E. Kay for providing pulse sequences; Gerry McQuaid for maintenance of the NMR spectrometers; J. Leigh Willard and Robert Boyko for computer expertise; Matt Crump for carefully reading the manuscript; and the Protein Engineering Network Centre of Excellence (PENCE) for the use of the Unity 600 NMR spectrometer.

SUPPORTING INFORMATION AVAILABLE

Three tables (S1, S2, and S3) showing acquisition parameters and pulse sequence details for ^{15}N relaxation experiments, and three figures (S1, S2, and S3), showing sensitivity-enhanced, nongradient pulse sequences for the measurement of ^{15}N-T_1, -T_2, and $\{^1H\}^{15}N$ NOE at 300 MHz (6 pages).

REFERENCES

1. Potter, J. D., and Gergely, J. (1975) *J. Biol. Chem. 250*, 4628−4633.
2. Zot, A. S., and Potter, J. D. (1987) *Annu. Rev. Biophys. Biophys. Chem. 16*, 535−559.
3. Grabarek, Z., Tao, T., and Gergely, J. (1992) *J. Muscle Res. Cell Motil. 13*, 383−393.
4. Farah, C. S., and Reinach, F. C. (1995) *FASEB J. 9*, 755−767.
5. Tobacman, L. S. (1996) *Annu. Rev. Physiol. 58*, 447−481.
6. Herzberg, O., and James, M. N. G. (1988) *J. Mol. Biol. 203*, 761−779.
7. Satyshur, K. A., Rao, S. T., Pyzalska, D., Drendal, W., Greaser, M., and Sundralingham, M. (1988) *J. Biol. Chem. 263*, 1628−1647.
8. Slupsky, C. M., and Sykes, B. D. (1995) *Biochemistry 34*, 15953−15964.
9. Negele, J. C., Dotson, D. G., Liu, W., Sweeny, H. L., and Putkey, J. A. (1992) *J. Biol. Chem. 267*, 825−831.
10. Putkey, J. A., Sweeny, H. L., and Campbell, S. T. (1989) *J. Biol. Chem. 264*, 12370−12378.
11. Putkey, J. A., Liu, W., and Sweeny, H. L. (1991) *J. Biol. Chem. 266*, 14881−14884.
12. Szczensna, D., Guzman, G., Millet, T., Zhao, J., Farokhi, K., Ellemberger, H., and Potter, J. D. (1996) *J. Biol. Chem. 271*, 8381−8386.
13. Gagné, S., Tsuda, S., Li, M. X., Smillie, L. B., and Sykes, B. D. (1995) *Nat. Struct. Biol. 2*, 784−789.
14. Herzberg, O., and James, M. N. G. (1985) *Nature 313*, 653−659.
15. Strynadka, N. C., Cherney, M., Sielecki, A. R., Li, M. X., Smillie, L. B., and James, M. N. (1997) *J. Mol. Biol. 273*, 238−255.
16. Houdusse, A., Love, M. L., Dominguez, R., Grabarek, Z., and Cohen, C. (1997) *Structure 5*, 1695−1711.
17. Spyracopoulos, L., Li, M. X., Sia, S. K., Gagné, S. M., Chandra, M., Solaro, R. J., and Sykes, B. D. (1997) *Biochemistry 36*, 12138−12146.
18. Sia, S. K., Li, M. X., Spyracopoulos, L., Gagné, S. M., Liu, W., Putkey, J. A., and Sykes, B. D. (1997) *J. Biol. Chem. 272*, 18216−18221.
19. van Eerd, J.-P., and Takahashi, K. (1975) *Biochem. Biophys. Res. Commun. 64*, 122−127.
20. Gagné, S. M., Li, M. X., and Sykes, B. D. (1997) *Biochemistry 36*, 4386−4392.
21. Li, M. X., Gagné, S. M., Tsuda, S., Kay, C. M., Smillie, L. B., and Sykes, B. D. (1995) *Biochemistry 34*, 8330−8340.
22. Li, M. X., Gagné, S. M., Spyracopoulos, L., Kloks, C. P. A. M., Audette, G., Chandra, M., Solaro, R. J., Smillie, L. B., and Sykes, B. D. (1997) *Biochemistry 36*, 12519−12525.
23. Wagner, G. (1993) *Curr. Opin. Struct. Biol. 3*, 748−753.
24. Palmer, A. G. (1993) *Curr. Opin. Biotechnol. 4*, 385−391.
25. Kay, L. E. (1998) *Nat. Struct. Biol. 5*, 513−517.
26. Lipari, G., and Szabo, A. (1982) *J. Am. Chem. Soc. 104*, 4546−4559.
27. Lipari, G., and Szabo, A. (1982) *J. Am. Chem. Soc. 104*, 4559−4570.
28. Kay, L. E., Torchia, D. A., and Bax, A. (1989) *Biochemistry 28*, 8972−8979.
29. Akke, M., Bruschweiler, R., and Palmer, A. G. (1993) *J. Am. Chem. Soc. 115*, 9832−9833.
30. Yang, D., and Kay, L. E. (1996) *J. Mol. Biol. 263*, 369−382.
31. Yang, D., Mok, Y.-K., Forman-Kay, J. D., Farrow, N. A., and Kay, L. E. (1997) *J. Mol. Biol. 272*, 790−804.
32. Gagné, S. M., Tsuda, S., Spyracopoulos, L., Kay, L. E., and Sykes, B. D. (1998) *J. Mol. Biol. 278*, 667−686.
33. Chandra, M., Dong, W.-J., Pan, B.-S., Cheung, H. C., and Solaro, R. J. (1997) *Biochemistry 36*, 13305−13311.
34. Gagné, S. M., Tsuda, S., Li, M. X., Chandra, M., Smillie, L. B., and Sykes, B. D. (1994) *Protein Sci. 3*, 1961−1974.
35. Golosinska, K., Pearlstone, J. R., Borgford, T., Oikawa, K., Kay, C. M., Carpenter, M. R., and Smillie, L. B. (1991) *J. Biol. Chem. 266*, 15797−15809.
36. Farrow, N. A., Muhandiram, R., Singer, A. U., Pascal, S. M., Kay, C. M., Gish, G., Shoelson, S. E., Pawson, T., Forman-Kay, J. D., and Kay, L. E. (1994) *Biochemistry 33*, 5984−6003.
37. Kördel, J., Skelton, N. J., Akke, M., Palmer, A. G., and Chazin, W. J. (1992) *Biochemistry 31*, 4856−4866.
38. Delaglio, F., Grzesiek, S., Vuister, G. W., Zhu, G., Pfeifer, J., and Bax, A. (1995) *J. Biomol. NMR 6*, 277−293.
39. Garrett, D. S., Powers, R., Gronenborn, A. M., and Clore, G. M. (1991) *J. Magn. Reson. 95*, 214−220.
40. Tjandra, N., Feller, S. E., Pastor, R. W., and Bax, A. (1995) *J. Am. Chem. Soc. 117*, 12562−12566.
41. Luginbühl, P., Pervushin, K. V., Iwai, H., and Wüthrich, K. (1997) *Biochemistry 36*, 7305−7312.
42. Lee, L. K., Rance, M., Chazin, W. J., and Palmer, A. G. (1997) *J. Biomol. NMR 9*, 287−298.
43. Tjandra, N., Kuboniwa, H., Ren, H., and Bax, A. (1995) *Eur. J. Biochem. 230*, 1014−1024.
44. Strynadka, N. C. J., and James, M. N. G. (1989) *Annu. Rev. Biochem. 58*, 951- 998.
45. Fischer, M. W. F., Zeng, L., Pang, Y., Hu, W., Majumdar, A., and Zuiderweg, E. R. P. (1997) *J. Am. Chem. Soc. 119*, 12629−12642.
46. Muhandiram, D. R., Yamazaki, T., Sykes, B. D., and Kay, L. E. (1995) *J. Am. Chem. Soc. 117*, 11536−11544.
47. Yang, D., Mittermaier, A., Mok, Y. K., and Kay, L. E. (1998) *J. Mol. Biol. 276*, 939−954.
48. Akke, M., Skelton, N. J., Kördel, J., Palmer, A. G., and Chazin, W. J. (1993) *Biochemistry 32*, 9832−9844.
49. Baldellon, C., Alattia, J.-R., Strub, M.-P., Pauls, T., Berchtold, M. W., Cavé, A., and Padilla, A. (1998) *Biochemistry 37*, 9964−9975.
50. Shaw, G. S., Hodges, R. S., and Sykes, B. D. (1990) *Science 249*, 280−283.
51. Kay, L. E., Forman-Kay, J. D., McCubbin, W. D., and Kay, C. M. (1991) *Biochemistry 30*, 4323−4333.
52. Monera, O. D., Shaw, G. S., Zhu, B.-Y., Sykes, B. D., Kay, C. M., and Hodges, R. S. (1992) *Protein Sci. 1*, 945−955.
53. Shaw, G. S., Hodges, R. S., and Sykes, B. D. (1992) *Biochemistry 31*, 9572−9580.
54. Shaw, G. S., and Sykes, B. D. (1996) *Biochemistry 35*, 7429−7438.
55. Evenäs, J., Thulin, E., Malmendal, A., Forsén, S., and Carlström, G. (1997) *Biochemistry 36*, 3448−3457.
56. Skoog, D. A. (1984) *Principles of Instrumental Analysis*, 3rd ed., Saunders College Publishing, Philadelphia, PA.
57. Carson, M. (1997) *Methods Enzymol. 277*, 493−505.

BI9816960